




This is the **accepted version** of the article:

Guster, Bogdan; Rubio Verdú, Carmen; Robles, Roberto; [et al.]. «Coexistence of elastic modulations in the charge density wave state of 2H-NbSe₂». Nano Letters, Vol. 19, issue 5 (May 2019), p. 3027-3032. DOI 10.1021/acs.nanolett.9b00268

This version is available at <https://ddd.uab.cat/record/215015>

under the terms of the  **IN** COPYRIGHT license

Coexistence of Elastic Modulations in the Charge Density Wave State of 2H-NbSe₂

*Bogdan Guster^{1,#}, Carmen Rubio-Verdú^{2,#}, Roberto Robles^{1,#}, Javier Zaldívar², Paul Dreher^{3,4},
Miguel Pruneda¹, José Ángel Silva-Guillén⁵, Deung-Jang Choi^{3,4,6}, José I. Pascual^{2,6}, Miguel M.
Ugeda^{*2,3,4,6}, Pablo Ordejón^{*1} and Enric Canadell^{*7}*

¹*Catalan Institute of Nanoscience and Nanotechnology (ICN2), CSIC and BIST, Campus UAB,
Bellaterra, 08193 Barcelona, Spain*

²*CIC nanoGUNE, 20018 San Sebastián, Spain*

³*Donostia International Physics Center (DIPC), Paseo Manuel de Lardizábal 5, 20018 San
Sebastián, Spain*

⁴*Centro de Física de Materiales (CSIC-UPV-EHU), Manuel Lardizábal 5, 20018 San Sebastián,
Spain.*

⁵*School of Physics and Technology, Wuhan University, Wuhan 430072, China*

⁶*Ikerbasque, Basque Foundation for Science, 48013 Bilbao, Spain*

⁷*Institut de Ciència de Materials de Barcelona (ICMAB-CSIC), Campus UAB, 08193 Bellaterra,
Spain*

*Corresponding authors: pablo.ordejon@icn2.cat, canadell@icmab.es and
mmugeda@dipc.org*

#These authors contributed equally.

Abstract. Bulk and single-layer $2H\text{-NbSe}_2$ exhibit identical charge density wave order (CDW) with a quasi-commensurate 3×3 superlattice periodicity. Here we combine scanning tunnelling microscopy (STM) imaging at $T = 1$ K of $2H\text{-NbSe}_2$ with first-principles density functional theory (DFT) calculations to investigate the structural atomic rearrangement of this CDW phase. Our calculations for single-layers reveal that six different atomic structures are compatible with the 3×3 CDW distortion, although all of them lie on a very narrow energy range of at most 3 meV *per* formula unit, suggesting the coexistence of such structures. Our atomically resolved STM images of bulk $2H\text{-NbSe}_2$ unambiguously confirm this by identifying two of these structures. Remarkably, these structures differ from the X-ray crystal structure reported for the bulk 3×3 CDW which, in fact, is also one of the six DFT structures located for the single-layer. Our calculations also show that due to the minute energy difference between the different phases, the ground state of the 3×3 CDW could be extremely sensitive to doping, external strain or internal pressure within the crystal. The presence of multi-phase CDW order in $2H\text{-NbSe}_2$ may provide further understanding of its low temperature state and the competition between different instabilities.

Keywords: Charge density waves, transition metal dichalcogenides, DFT calculations, $2H\text{-NbSe}_2$, STM.

Main text.

The genuine origin of the charge density wave (CDW) state in NbSe_2 has been a matter of continuous debate.^{1,2} Clearing up this point is an unavoidable issue in any attempt to understand the interplay between CDW and superconducting (SC) states in this paradigmatic material.³ Bulk $2H\text{-NbSe}_2$ is a room temperature metal which at 33 K undergoes a transition towards an atypical CDW state⁴ with practically no resistivity change through the transition. Below 33 K the system exhibits a modulated almost quasi-commensurate 3×3 structure⁵ and at 7 K enters into a SC state⁶. It has been recently shown that the CDW order remains intact in single-layer NbSe_2 .⁷ In contrast with $2H\text{-NbSe}_2$, the CDW modulation in bulk $2H\text{-TaSe}_2$ is 3×3 commensurate at low temperature.⁵ Dichalcogenides of the $2H\text{-MX}_2$ family provide promising playground for the study of

1
2
3 competing electronic instabilities in the 2D limit, $2H\text{-NbSe}_2$ being specially challenging
4 because of the incommensurability of its CDW.
5

6 Single-layers of $2H\text{-NbSe}_2$ (from now on we will refer to them simply as NbSe_2) are
7 hexagonal layers of Nb atoms in a trigonal prismatic environment of Se atoms (Figure 1a).⁸
8 Although the superlattice periodicity (quasi-commensurate 3×3) has been accurately
9 measured,⁵ the microscopic structure of the elastic distortion that accompanies the CDW
10 phase still remains elusive. The layers of bulk $2H\text{-NbSe}_2$ were recently found to exhibit a
11 continuous pattern of overlapping star-shaped Nb atom clusters extending along the layer.⁹
12 More recently, a first-principles DFT study on single-layer NbSe_2 assuming a
13 commensurate 3×3 modulation revealed that several structures with nearly equal stability
14 but different distortion patterns are compatible with a 3×3 modulation.¹⁰ This suggests a
15 very flat potential energy surface and a plausible coexistence of the different modulations.
16 This potentiality apparently stimulated two subsequent theoretical works.^{11,12} However, a
17 comprehensive picture of the exact elastic modulations cannot be solved from a purely
18 theoretical DFT approach since (i) the real modulation is strictly non-commensurate, and
19 (ii) the resulting competing modulations have very similar energetic stability. Because of
20 the simultaneous occurrence of these two features, theoretically optimized 3×3
21 commensurate structures can only be taken as suggestions of different possibilities to be
22 carefully examined by suitable experimental techniques. STM well suits for this purpose
23 since it can image with atomic resolution the spatial rearrangement of the electronic charge
24 of the CDW phase. Such electronic rearrangements can be compared to those simulated for
25 the different calculated elastic modulations. Here we report a combined experimental-
26 theoretical study to provide compelling evidence for the coexistence of different
27 modulations in the CDW state of NbSe_2 . In order to search for the several possible
28 competing phases, we perform total energy minimizations starting from different distorted
29 starting configurations. Some of the structures were only found when a charge doping was
30 initially considered. Once such structures are located for a given doping value, their
31 evolution with doping was also followed. While some of the phases were found for the
32 whole range of doping considered, others were observed for some doping intervals. Doping
33 is therefore used as a practical way to unravel competing structures in our calculations.
34 Nevertheless, we note that our results of the stability of the several structures as a function
35
36
37
38
39
40
41
42
43
44
45
46
47
48
49
50
51
52
53
54
55
56
57
58
59
60

of doping can also be relevant to experiments where injection of carriers in the single layers is achieved through electric field gating.¹³ We also note again that our commensurate 3×3 structural models are only (close) approximations to the true experimental incommensurate structures.

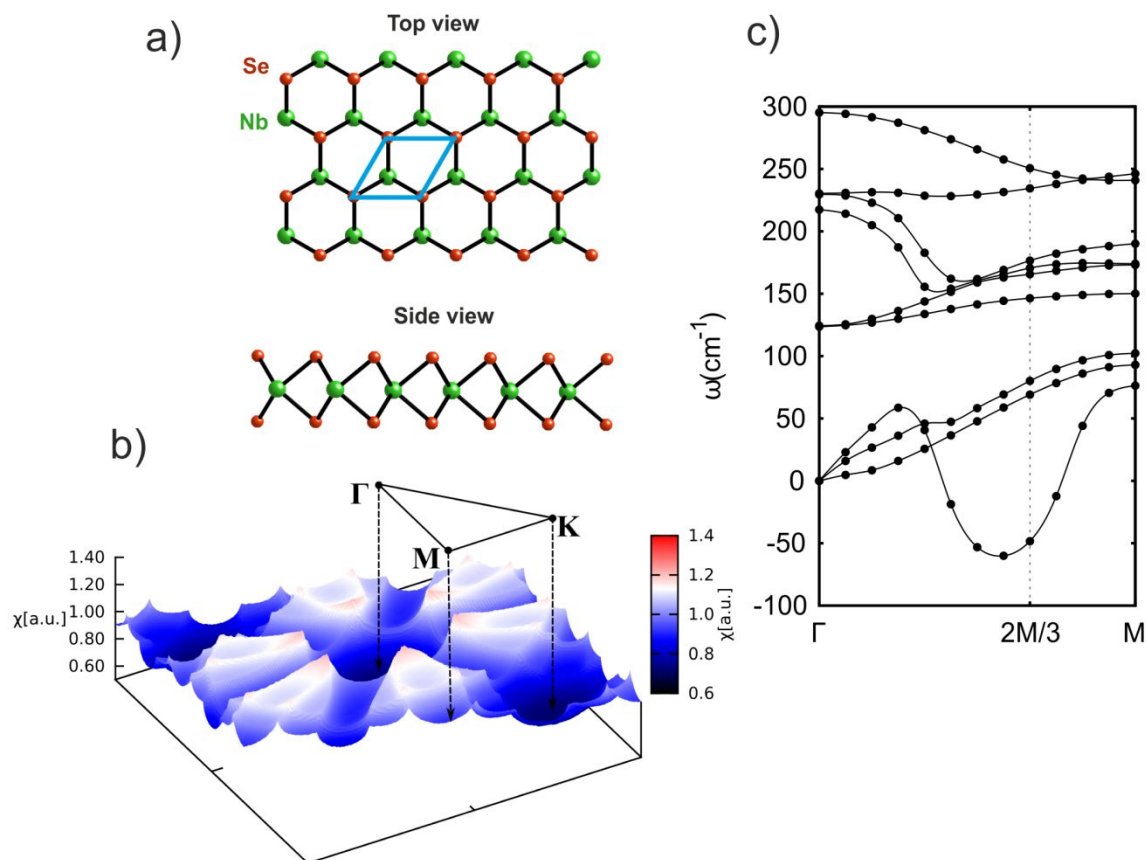


Figure 1: (a) Top and side view of the NbSe₂ single-layer structure. Lindhard response function (b) and (c) phonon dispersion in the Γ - M segment of the Brillouin zone calculated for undistorted single-layer NbSe₂.

Full optimization of the non-modulated structure of single-layer NbSe₂ leads to a lattice constant of 3.48 Å, in good agreement with plane-wave type DFT studies,¹¹ 3.47 Å,

1
2
3 and the experimental value for the bulk, 3.44 Å.⁸ The band structure and Fermi surface of
4 single-layer NbSe₂ in both modulated¹⁰⁻¹² and non modulated¹⁴⁻¹⁶ structures have been
5 discussed before. Such Fermi surface contains rounded hexagons and rounded triangles
6 centered at Γ and K points of the Brillouin zone (BZ), respectively. The calculated
7 Lindhard response function for the optimized non modulated single-layer NbSe₂ is shown
8 in Figure 1b. As it occurs for the bulk,¹⁷ there are no sharp maxima around the $(a^*/3, 0)$
9 point and equivalent ones of the BZ which could justify a Fermi surface nesting driven
10 mechanism of the CDW, but a very shallow region around the Γ - M direction. In contrast,
11 as can be seen in the phonon band structure of the optimized non modulated structure
12 shown in Figure 1c, one of the phonon branches becomes clearly unstable in a large part of
13 the Γ -M segment of the BZ, with a maximum imaginary frequency near but not exactly at
14 the $a^*/3$ point. The presence of phonons with imaginary frequency around this point
15 indicates that the system is unstable with respect to incommensurate distortions with a
16 periodicity not far from 3×1 (and symmetry equivalent). The combination of the three
17 equivalent distortions (threefold symmetry, i.e. triple-q or 3Q mechanism), leads to an
18 incommensurate structure close to 3×3 . We conclude that the modulation of the single-layer
19 NbSe₂ is a strong-coupling CDW caused by electron-phonon coupling, as it has been
20 proposed for the bulk¹⁶ and we previously discussed for single-layers.¹⁰

21
22 We then performed structural optimizations imposing a 3×3 periodicity for the pristine
23 as well as for several doping levels of single-layer NbSe₂. We also checked that the phonon
24 instability remains under doping: as we show in the Supplementary Information, the effect
25 of doping does not change this picture qualitatively, although the precise shape of the
26 unstable phonon branch and the position of the minimum experience some small changes.
27 A summary of this study is reported in Figure 2. Up to six different modulations compatible
28 with a 3×3 cell were found. One of the structures exhibits centered hexagonal clusters of
29 Nb atoms and single Nb atoms in between (noted Hexagons in Figure 2). Another structure
30 contains a continuous pattern of overlapping star-shaped Nb atom clusters (noted Stars in
31 Figure 2) which coincides with the 3×3 modulation reported for the bulk.⁹ Two structures
32 contain triangular clusters of 3 and 6 Nb atoms (T1 and T1' in Figure 2) but whereas in T1
33 the inner triangles of both clusters are centered by two Se atoms above and below the Nb
34 atoms plane, in T1' they are centered by hollows. Finally, two more structures contain a
35
36
37
38
39
40
41
42
43
44
45
46
47
48
49
50
51
52
53
54
55
56
57
58
59
60

1
2
3 continuous pattern of overlapping triangular clusters of 6 Nb atoms of two different types,
4 with or without Nb-Nb short distances inside the large triangles (T2 and T2' in Figure 2).
5 Note that the six structures can be paired in three groups: Hexagons/Stars, T1/T2 and
6 T1'/T2' so that within each pair the short and long Nb-Nb bonds are interchanged. This
7 suggests that the two structures within each pair may be interconverted as a function of
8 doping. This is indeed the case for the T1/T2 and T1'/T2' pairs where a relatively simple
9 gradual change between the two structures is possible. However, the Hexagons/Stars pair
10 could not be exchanged due to their complex arrangement. Consequently, for a given
11 carrier-density there are four different structures compatible with a 3×3 modulation.
12 Remarkably, for most doping levels the energy difference between these structures is
13 extremely small (between fractions of a meV and at most 2 meV) so that it is likely that
14 some of the structures experimentally coexist. Let us stress that our calculations are carried
15 out for a commensurate 3×3 CDW structure but the real modulation is incommensurate. As
16 a consequence of this fact and the very small energy differences, the data in Figure 2a
17 should be only taken as suggesting that some of these structures may coexist in real
18 samples and weak changes in doping, strain or internal pressure of the crystal may alter
19 such coexistence.
20
21
22
23
24
25
26
27
28
29
30
31
32
33
34
35
36
37
38
39
40
41
42
43
44
45
46
47
48
49
50
51
52
53
54
55
56
57
58
59
60

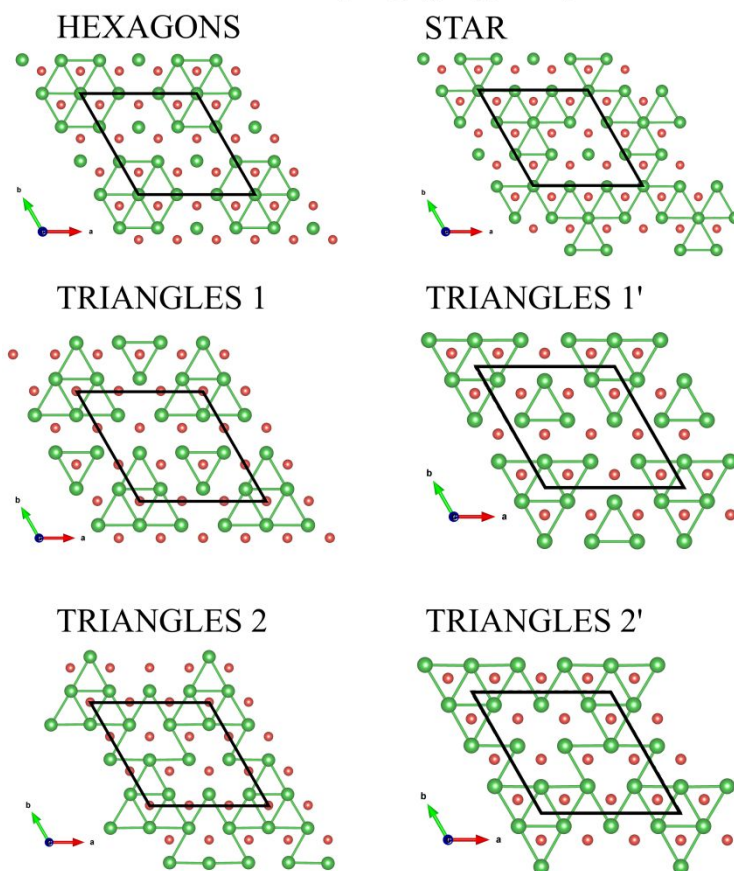
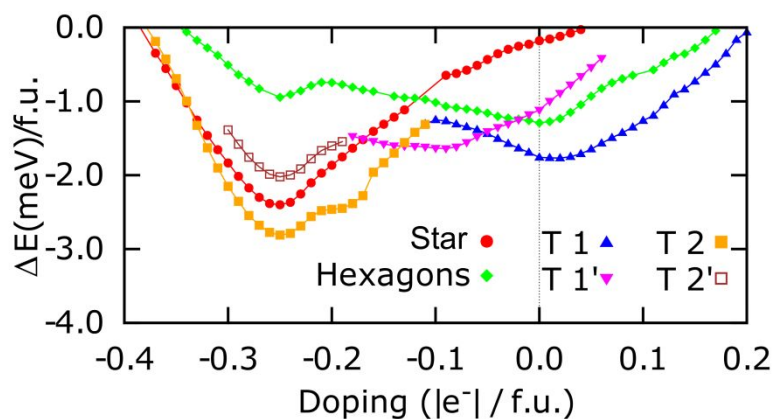


Figure 2: Different modulations compatible with a 3×3 periodicity and their relative energies for single-layer NbSe_2 as a function of external doping (in electrons per formula unit; negative values indicate electron doping). For a given doping value the energy (in meV *per* formula unit) is given with respect to the optimized non distorted system for the same doping level. Nb-Nb contacts shorter than in the average structure are those shown in the structural drawings. Nb-Nb bonds smaller than the lattice constants are marked with green lines to visualize the different modulations.

1
2
3
4
5 We have performed the analysis of the stability of the six different structures with 3×3
6 periodicity by obtaining the phonon frequencies. As some of the phases are only stable
7 under charge doping, the frequencies were obtained using two doping values: 0 and -0.25
8 e/f.u. For no doping, we find that the hexagons, T1 and T1' structures are stable and show
9 no imaginary frequencies, while the stars phase does show three imaginary frequencies, in
10 agreement with the previous works.^{11,12} For the case of -0.25 e/f.u. doping, we find that the
11 T2, T2' and stars phases are stable, while the hexagons phase has three imaginary
12 frequencies. We note that this is consistent with the energy ordering of the phases as a
13 function of doping in Figure 2: the phases which are found to have unstable modes are the
14 ones with higher energies (stars for zero doping, and hexagons for -0.25 e/f.u. doping).

15
16
17
18
19
20
21
22 In order to experimentally explore the existence of these structural phases, we have
23 imaged the surface of bulk $2H\text{-NbSe}_2$ with atomic resolution by means of scanning
24 tunnelling microscopy (STM) at $T = 1$ K. Since both bulk and single-layer NbSe_2 exhibit
25 the same 3×3 CDW phase,⁷ we carried out our experiments in its bulk form due to its
26 much lower density of defects (grain boundaries and domain edges are not present in bulk),
27 which might alter the energy landscape of the CDW phases. Furthermore, the purely two
28 dimensional character of the CDW order in NbSe_2 allows us to directly probe the existence
29 of the structural phases predicted for single-layer NbSe_2 in the bulk form. The analysis of
30 tens of different regions of bulk NbSe_2 led to identification of two different structural
31 phases. Upper panel in Figure 3 shows two STM images of a representative region for
32 unoccupied (Figure 3a) and occupied (Figure 3b) states. The STM images reveal the
33 coexistence of two different phases (depicted in blue/yellow) separated by an Å-scale
34 boundary (black dashed line). Although the two phases show the same 3×3 superlattice
35 periodicity at both polarities, the relative intensity of the nine Se atoms of each 3×3 unit
36 cell (blue and yellow cells) vary differently, thus giving rise to a unique pattern in each
37 case. Figures 3c-f show close-up views of these patterns for the two phases at each polarity.
38 Such unique patterns allowed us to compare both structural phases with simulated STM
39 images from the six stable structures, within the Tersoff-Hamann approximation pattern
40 (see the Supplementary Information for the images of the Hexagons, Stars and T1' phases
41 not shown in Figure 3).¹⁸ As a first result, the experimental phase labelled in blue can be
42
43
44
45
46
47
48
49
50
51
52
53
54
55
56
57
58
59
60

1
2
3 identified with the theoretical T2'. Figures 3g and 3i show the simulated STM images of
4 this phase at ± 0.05 V that compare with the experimental STM images in Figures 3c and
5 3e, respectively. The theoretical 3×3 unit cells reproduce the relative intensity of the Se
6 atoms within the unit cells simultaneously for both polarities as well as their relative
7 orientation. Regarding the yellow phase, it can be identified with either the T1 or T2 phases
8 since they exhibit almost the same patterns at both polarities and, therefore, are practically
9 indistinguishable. Figures 3h and 3j show the simulated STM images for the T1 phase at \pm
10 0.05 V (those for T2 are almost identical) for comparison with the experimental ones in
11 Figures 3d and 3f, respectively. Here, again, the patterns within the 3×3 unit cells show a
12 good agreement between theory and experiment. We therefore assign the observed yellow
13 (blue) phases to the T2' and T1/T2 phases. Although this is the most likely correspondence
14 between the experimental and theoretical phases, the blue phase can also be identified as
15 the Stars phase according to the superlattice. However, this would imply a rotation of 180°
16 of the crystal lattice with respect to the T1/T2 phase and, therefore, their mutual
17 coexistence is not compatible in light of the experimental data.
18
19

20
21 In summary, on the basis of first-principles DFT calculations six different structures
22 are found to be compatible with the 3×3 CDW structure of NbSe₂. All these structures are
23 found to coexist in a very narrow energy range of 2-3 meV. Their relative stability can be
24 subtly altered by doping or strain. Imaging the surface of bulk 2H-NbSe₂ with atomic
25 resolution allowed us to identify two of these structures, as anticipated by our theoretical
26 simulations. Intriguingly, these structures differ from the X-ray crystal structure reported
27 for the bulk 3×3 CDW⁹ which, in fact, is also one of the six DFT structures located for the
28 single-layer (Stars in Figure 2). Preliminary calculations for slabs with a different number
29 of layers suggest that the actual structure stabilized may change from layer to layer, i.e., the
30 energetic preference may depend also on the internal pressure. The coexistence of different
31 structures in 2H-NbSe₂ has far-reaching consequences to fully understand the electronic
32 ground state of 2H-NbSe₂. Thus, experimental work on slabs with different number of
33 layers is encouraged since it may provide important clues to understand the puzzling
34 physics of this correlated material.
35
36
37
38
39
40
41
42
43
44
45
46
47
48
49
50
51
52
53
54
55
56
57
58
59
60

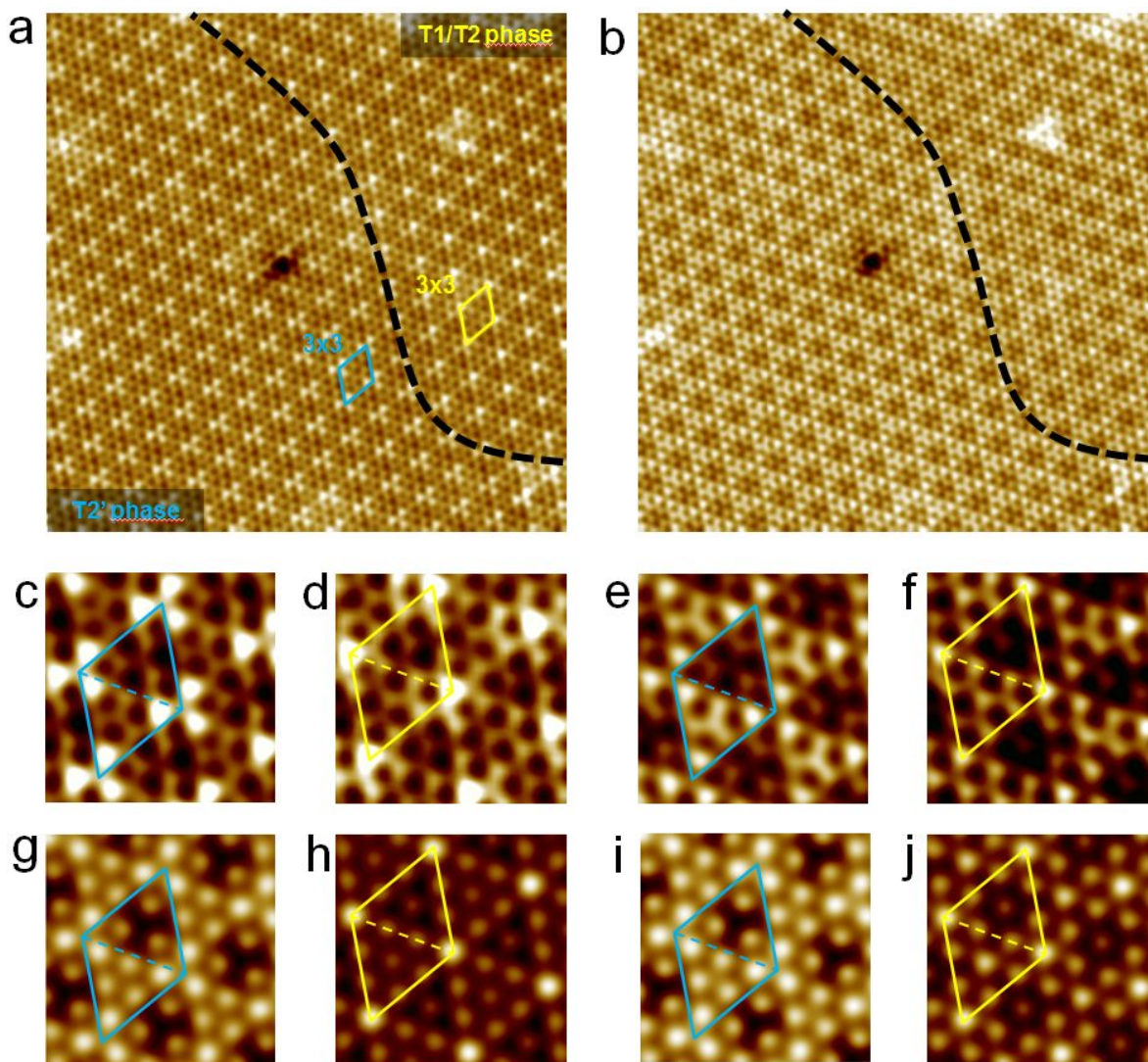


Figure 3. Unoccupied [+50 mV] (a) and occupied [-50 mV] (b) STM images (14 nm x 14 nm) of the same region of bulk $2H\text{-NbSe}_2$ showing the coexistence of two structural phases. The black dashed line represents the boundary between them. Parameters: (a) $V_S = 50$ mV, $I = 0.5$ nA and (b) $V_S = -50$ mV, $I = 0.5$ nA. (c-f) Zoom-in STM images from **a** and **b** of the two phases for unoccupied (c,d) and occupied (e,f) states. (g-j) Simulated STM images for both phases and bias polarities ($V_S = \pm 50$ mV).

Computational details. The geometrical optimizations, electronic and phonon band structures were carried out with density functional theory (DFT)^{19,20} using a numerical

1
2
3 atomic orbitals approach implemented in the SIESTA code.^{21,22} We used the Perdew-Burke-
4 Ernzerhof (PBE) functional to account for the exchange-correlation energy.²³ A split-
5 valence double- ζ basis set²⁴ was used to describe the valence electrons wave function, while
6 the core electrons were replaced by norm conserving scalar relativistic pseudopotentials²⁵
7 factorized in the Kleinman-Bylander form.²⁶ The 4p shell of Nb was included in the
8 valence explicitly as semicore states. For a good description of the free standing layer, we
9 placed the single layer in a vacuum space of 50 Å to avoid interactions between the layer
10 and its images. We used an energy cutoff of 2500 Ry for the real space integration. A
11 tolerance of 10^{-5} and 10^{-4} on the density matrix and total energy, respectively, was used in
12 order to attain the convergence of the self-consistency cycle. Geometrical optimization
13 calculations were performed to ensure a maximum atomic force of 4×10^{-3} eV/Å⁻¹. A
14 Monkhorst-Pack²⁷ k -point grid of $72 \times 72 \times 1$ was used to account for the sampling of the
15 Brillouin zone of the minimum unit cell and it was scaled accordingly where supercell
16 calculations were performed. Phonon calculations were done using the finite difference
17 method. In the case of the phonon band structure calculations, a k -point grid of $120 \times 120 \times 1$
18 per minimum unit cell and a 5×10^{-3} eV Fermi-Dirac smearing were used.
19
20
21
22
23
24
25
26
27
28
29
30

31
32 **Experimental details.** Bulk NbSe₂ crystals were cleaved under Ultra-High Vacuum
33 (UHV) conditions, and subsequently transferred *in-situ* into a SPECS GmbH Low-
34 Temperature STM for imaging at T = 1.2 K. STM/STS analysis and rendering was done
35 using the WSxM software.²⁸
36
37
38
39

40 41 **ORCID**

42 Bogdan Guster: 0000-0003-1305-1862

43 Roberto Robles: 0000-0001-7808-0395

44 Enric Canadell: 0000-0002-4663-5226

45 Pablo Ordejón: 0000-0002-2353-2793

46 José Ángel Silva-Guillen: 0000-0002-0483-5334

47 José Ignacio Pascual: 0000-0002-7152-4747
48
49
50
51
52
53
54
55
56
57
58
59
60

Notes

The authors declare no competing financial interest.

Acknowledgements. Work at Bellaterra was supported by Spanish MINECO (Grants FIS2015-64886-C5-3-P and FIS2015-64886-C5-4-P, and the Severo Ochoa Centers of Excellence Program under Grants SEV-2017-0706 and SEV-2015-0496), Generalitat de Catalunya (Grant 2017SGR1506 and the CERCA Program) and by the European Union MaX Center of Excellence (Grant No. 824143). The work by BG has been performed in the context of the Physics PhD program of the Universitat Autònoma de Barcelona. M.M.U acknowledges support by the Spanish MINECO under grant no. MAT2017-82074-ERC and by the ERC Starting grant “LINKSPM” (Grant No. 758558).

References

1. Rossmagel, K. On the origin of charge-density waves in select layered transition-metal dichalcogenides. *J. Phys.:Cond. Matt.* **2011**, *23*, 213001.
2. Zhu, X.; Cao, Y.; Zhang, J.; Plummer, E. W.; Guo, J. Classification of charge density waves based on their nature. *Proc. Nat. Acad. Sci. USA* **2018**, *112*, 2367.
3. Castro Neto, A. H. Charge Density Wave, Superconductivity, and Anomalous Metallic Behavior in 2D Transition Metal Dichalcogenides. *Phys. Rev. Lett.* **2001**, *86*, 4382.
4. Wilson, J.; Di Salvo, F.; Mahajan, S. Charge-density waves and superlattices in the metallic layered transition metal dichalcogenides. *Adv. Phys.* **1975**, *24*, 117-201.
5. Moncton, D. E.; Axe, J. D.; DiSalvo, F. J. Neutron scattering study of the charge-density wave transitions in 2H-TaSe₂ and 2H-NbSe₂. *Phys. Rev. B* **1977**, *16*, 801.
6. Revolinsky, E.; Lautenschlager, E. P.; Armitage, C. H. Layer structure superconductor. *Solid State Comm.* **1963**, *1*, 59-61.
7. Ugeda, M. M. ; Bradley, A. J.; Zhang, Yi; Onishi, S.; Chen, Yi; Ruan, W.; Ojeda-Aristizabal, C.; Ryu, H.; Edmons, M. T.; Tsai, H.-Z.; Riss, A.; Mo, S.-K.; Lee, D.; Zettl, A.; Hussain, Z.; Shen, Z.-X.; Crommie, M. F. Characterization of collective ground states in single-layer NbSe₂. *Nature Phys.* **2016**, *12*, 92.

- 1
 - 2
 - 3
 - 4
 - 5
 - 6
 - 7
 - 8
 - 9
 - 10
 - 11
 - 12
 - 13
 - 14
 - 15
 - 16
 - 17
 - 18
 - 19
 - 20
 - 21
 - 22
 - 23
 - 24
 - 25
 - 26
 - 27
 - 28
 - 29
 - 30
 - 31
 - 32
 - 33
 - 34
 - 35
 - 36
 - 37
 - 38
 - 39
 - 40
 - 41
 - 42
 - 43
 - 44
 - 45
 - 46
 - 47
 - 48
 - 49
 - 50
 - 51
 - 52
 - 53
 - 54
 - 55
 - 56
 - 57
 - 58
 - 59
 - 60
8. Meerschaut, A.; Deudon, C. Crystal structure studies of the 3R-Nb_{1.09}S₂ and 2H-NbSe₂ compounds: correlation between nonstoichiometry and stacking type (= polytypism). *Mat. Res. Bull.* **2001**, *36*, 1721-1727.
9. Malliakas, C. D.; Kanatzidis, M. G. Nb-Nb Interactions Define the Charge Density Wave Structure of 2H-NbSe₂. *J. Am. Chem. Soc.* **2013**, *135*, 1719-1722.
10. Silva-Guillén, J. A.; Ordejón, P.; Guinea, F.; Canadell, E. Electronic structure of 2H-NbSe₂ single-layers in the CDW state. *2D Materials* **2016**, *3*, 035028.
11. Zheng, F.; Zhou, Z.; Liu, X.; Feng, J. First-principles study of charge and magnetic ordering in monolayer NbSe₂. *Phys. Rev. B* **2018**, *97*, 081101(R).
12. Lian, C.-S.; Si, C.; Duan, W. Unveiling Charge-Density Wave, Superconductivity, and Their Competitive Nature in Two-Dimensional NbSe₂. *Nano Lett.* **2018**, *18*, 2924.
13. Note that doping of transition metal dichalcogenide single-layers can also be achieved by growing the single-layers on a Au(111) substrate: (a) Sanders, C. E.; Dendzik, M.; Ngankeu, A. S.; Eich, A.; Bruix, A.; Bianchi, M.; Miwa, J. A.; Hammer, B.; Khajetoorians, A. A.; Hofmann, P. Crystalline and electronic structure of single-layer TaS₂. *Phys. Rev. B* **2016**, *94*, 081404; (b) Albertini, O. R.; Liu, A. Y.; Calandra, M. Effect of electron doping on lattice instabilities in single-layer 1H-TaS₂. *Phys. Rev. B* **2017**, *95*, 235121.
14. Kim, S.; Son, Y.-W. Quasiparticle energy bands and Fermi surfaces of monolayer NbSe₂. *Phys. Rev. B* **2017**, *96*, 155439.
15. Lebègue, S.; Eriksson, O. Electronic structure of two-dimensional crystals from *ab initio* theory. *Phys. Rev. B* **2009**, *79*, 115409.
16. Calandra, M.; Mazin, I. I.; Mauri, F. Effect of Dimensionality on the charge-density wave in few-layer 2H-NbSe₂. *Phys. Rev. B* **2009**, *80*, 241108.
17. Johannes, M. D.; Mazin, I. I.; Howells, C. A. Fermi-surface nesting and origin of the charge-density wave in NbSe₂. *Phys. Rev. B* **2006**, *73*, 205102, and references therein.
18. Tersoff, J.; Hamman, D. R. Theory and Application for the Scanning Tunneling Microscope. *Phys. Rev. Lett.* **1983**, *50*, 1998.
19. Hohenberg, P.; Kohn, W. Inhomogeneous Electron Gas. *Phys. Rev.* **1964**, *136*, B864-B871.

- 1
 - 2
 - 3
 - 4
 - 5
 - 6
 - 7
 - 8
 - 9
 - 10
 - 11
 - 12
 - 13
 - 14
 - 15
 - 16
 - 17
 - 18
 - 19
 - 20
 - 21
 - 22
 - 23
 - 24
 - 25
 - 26
 - 27
 - 28
 - 29
 - 30
 - 31
 - 32
 - 33
 - 34
 - 35
 - 36
 - 37
 - 38
 - 39
 - 40
 - 41
 - 42
 - 43
 - 44
 - 45
 - 46
 - 47
 - 48
 - 49
 - 50
 - 51
 - 52
 - 53
 - 54
 - 55
 - 56
 - 57
 - 58
 - 59
 - 60
20. Kohn, W.; Sham, L. J. Self-Consistent Equations Including Exchange and Correlation Effects. *Phys. Rev.* **1965**, *140*, A1133-A1138.
21. Soler, J. M.; Artacho, E.; Gale, J. D.; García, A.; Junquera, J.; Ordejón, P.; Sánchez-Portal, D. The SIESTA method for ab initio order-N materials simulation. *J. Phys.: Cond. Matt.* **2002**, *14*, 2745-2779.
22. Artacho, E.; Anglada, E.; Diéguez, O.; Gale, J. D.; García, A.; Junquera, J.; Martín, R. M.; Ordejón, P.; Pruneda, J. M.; Sánchez-Portal, D.; Soler, J. M. The SIESTA method: developments and applicability. *J. Phys. Cond. Matter* **2008**, *20*, 064208.
23. Perdew, J. P.; Burke, K.; Ernzerhof, M. Generalized Gradient Approximation Made Simple. *Phys. Rev. Lett.* **1996**, *77*, 3865-3868.
24. Artacho, E.; Sánchez-Portal, D.; Ordejón, P.; García, A.; Soler, J. M. Linear Scaling ab-initio Calculations for Large and Complex Systems. *Phys. Status Solidi B* **1999**, *215*, 809-817.
25. Troullier, N.; Martins, J. L. Efficient Pseudopotentials for plane-wave calculations. *Phys. Rev. B* **1991**, *43*, 1993-2006.
26. Kleinman, L.; Bylander, D. M. Efficacious Form for Model Pseudopotentials. *Phys. Rev. Lett.* **1982**, *48*, 1425-1428.
27. Monkhorst, H. J.; Pack, Special points for Brillouin zone integrations. *J. D. Phys. Rev. B* **1976**, *13*, 5188-5192.
28. Horcas, I.; Fernández, R. WSXM: A software for scanning probe microscopy and a tool for nanotechnology. *Rev. Sci. Instrum.* **2007**, *78*, 013705.

For the Table of Contents

